

Type II Cepheids in the Milky Way disc[★]

Chemical composition of two new W Vir stars: DD Vel and HQ Car

B. Lemasle¹, V. Kovtyukh², G. Bono³, P. François^{4,5}, I. Saviane⁶, I. Yegorova⁶, K. Genovali³, L. Inno^{3,7},
G. Galazutdinov^{8,9}, and R. da Silva³

¹ Anton Pannekoek Institute for Astronomy, University of Amsterdam, Science Park 904, PO Box 94249, 1090 GE, Amsterdam, The Netherlands, e-mail: B. J. P. Lemasle@uva.nl

² Astronomical Observatory, Odessa National University, and Isaac Newton Institute of Chile, Odessa branch, Shevchenko Park, 65014, Odessa, Ukraine

³ Dipartimento di Fisica, Università di Roma Tor Vergata, via della Ricerca Scientifica 1, 00133 Rome, Italy

⁴ GEPI, Observatoire de Paris, CNRS, Université Paris Diderot, Place Jules Janssen, 92190 Meudon, France

⁵ UPJV-Université de Picardie Jules Verne, 80000 Amiens, France

⁶ European Southern Observatory, Alonso de Cordova 3107, Santiago, Chile

⁷ European Southern Observatory, Karl-Schwarzschild-Str. 2, D-85748 Garching bei Munchen, Germany

⁸ Instituto de Astronomia, Universidad Catolica del Norte, av. Angamos 0610, Antofagasta, Chile

⁹ Pulkovo Observatory, Pulkovskoe Shosse 65, Saint-Petersburg 196140, Russia

Received September 15, 1996; accepted March 16, 1997

ABSTRACT

Context. A robust classification of Cepheids into their different sub-classes and, in particular, between classical and Type II Cepheids, is necessary to properly calibrate the period-luminosity relations and for populations studies in the Galactic disc. Type II Cepheids are, however, very diverse, and classifications based either on intrinsic (period, light curve) or external parameters (e.g., [Fe/H], [Z]) do not provide a unique classification.

Aims. We want to ascertain the classification of two Cepheids, HQ Car and DD Vel, that are sometimes classified as classical Cepheids and sometimes as Type II Cepheids.

Methods. To achieve this goal, we examine both their chemical composition and the presence of specific features in their spectra.

Results. We find emission features in the H α and in the 5875.64 Å He I lines that are typical of W Vir stars. The [Na/Fe] (or [Na/Zn]) abundances are typical of thick-disc stars, while BL Her stars are Na-overabundant ([Na/Fe] > +0.5 dex). Finally, the two Cepheids show a possible (HQ Car) or probable (DD Vel) signature of mild dust-gas separation that is usually observed only in long-period type II Cepheids and RV Tau stars.

Conclusions. These findings clearly indicate that HQ Car and DD Vel are both Type II Cepheids from the W Vir sub-class. Several studies have reported an increase in the Cepheids' abundance dispersion towards the outer (thin) disc. A detailed inspection of the Cepheid classification, in particular for those located in the outer disc, will indicate whether this feature is real or simply an artefact of the inclusion of type II Cepheids belonging to the thick disc in the current samples.

Key words. stars: abundances - stars: atmospheres - stars: variables: Cepheids

1. Introduction

Type II Cepheids are the older, fainter, low-mass counterpart to the classical Cepheids (e.g., Wallerstein 2002). As such, they fall into the instability strip between the RR Lyrae and the RV Tau stars, and their periods are bound to ≈ 1 day on the lower end and to ≈ 20 days on the upper end, following the classification of Soszyński et al. (2008b). However, the limit between RR Lyrae and Type II Cepheids, on the one hand, and between Type II Cepheids and RV Tau stars, on the other, are not clearly defined. Type II Cepheids are themselves divided in two sub-classes; the BL Her stars have periods ranging from ≈ 1 to ≈ 4 days while the W Vir stars have periods between ≈ 4 and ≈ 20 days, again according to Soszyński et al. (2008b). In our current understanding, the different classes correspond to

stars in different evolutionary stages: BL Her stars are currently evolving from the horizontal branch (HB) to the asymptotic giant branch (AGB) and can be considered as post early-AGB stars (Castellani et al. 2007). W Vir stars cross the instability strip in their so-called “blue-nose” from the AGB while they are undergoing He-shell flashes. Finally, RV Tau stars are about to leave the AGB, so they are crossing the instability strip towards the white dwarf domain (Gingold et al. 1985; Bono et al. 1997, and references therein; see also Maas et al. (2007) for further considerations).

Various criteria have been tested to distinguish between classical and Type II Cepheids, and among the Type II Cepheids, to distinguish the BL Her and the W Vir stars. They are based on the shape of the light curve, on the stability of the period, or on the presence of distinctive features in the spectra. If these criteria have proved to be useful (see for instance Schmidt et al. 2004a), they are not sufficient to secure a robust classification.

[★] Based on observations collected at the European Organisation for Astronomical Research in the Southern Hemisphere, Chile (prog. ID: 060.A-9120 and 082.D-0901)

Indeed for various criteria, the properties of different types of variables overlap over various period ranges (e.g., Schmidt et al. 2005b; Soszyński et al. 2008b). Moreover, the use of external parameters (metallicity, proper motion, distance to the Galactic plane) is hampered by the fact that Type II Cepheids are very heterogeneous, because they span a wide metallicity range, and they can be found in the bulge, the thick disc, the halo, or in globular clusters.

The difficulty for properly classifying the Type II Cepheids can be illustrated by the two stars in our sample: DD Vel and HQ Car. DD Vel is classified as a classical Cepheid pulsating in the fundamental mode in the ASAS catalogue (Pojmanski 2002) and in the Machine-learned ASAS Classification Catalog (MACC, Richards et al. 2012) but as a Type II Cepheid in both the General Catalog of Variable Stars (GCVS, Samus et al. 2007-2013) and in the International Variable Star Index (VSX, Watson 2006). It is not listed as a Type II Cepheid by Harris (1985). HQ Car is considered as a classical Cepheid in the GCVS and in both the ASAS and MACC catalogues, while it is listed as a Type II Cepheid by Harris (1985) and in the VSX. It is worth mentioning that neither of the two stars is listed in the Fernie database of classical Cepheids (Fernie et al. 1995).

Surprisingly, Type II Cepheids did not receive much attention (see references in Maas et al. 2007) after the early spectroscopic analyses of Rodgers & Bell (1963, 1968), Barker et al. (1971), and Anderson & Kraft (1971). Indeed, modern high resolution spectroscopic studies have been limited to only a few stars: TX Del (Andrievsky et al. 2002), ST Pup (Gonzalez & Wallerstein 1996), V553 Cen (Wallerstein & Gonzalez 1996), and RT Tra (Wallerstein et al. 2000) before Maas et al. (2007) analysed 19 BL Her and W Vir stars. The study of Maas et al. (2007) is, to date, the unique extensive abundance analysis of Type II Cepheids. Amongst other results, they made three significant points regarding the classification of Type II Cepheids:

- Amongst stars with short periods, there is a clear separation into two groups. The BL Her stars are relatively metal-rich and show excesses of sodium, carbon, and nitrogen, along with thick disc kinematics. The UY Eri stars are significantly more metal-poor and are similar to stars in the halo;
- Stars with periods between 10 and 20 days, such as W Vir itself, show metallicities ranging approximately from -1.0 to -2.0 and are similar to variables in globular clusters;
- Stars with periods longer than 20 days show element separation as do RV Tau stars. A few stars with periods in the 20–30 day range, such as TW Cap, are as metal-poor as the 10–20-day stars.

Since the Maas et al. (2007) paper, only two new Type II Cepheids have been studied in detail: QQ Per by Wallerstein et al. (2008) and W Vir by Kovtyukh et al. (2011).

After a brief description of the data in Sect. 2, we examine in Sect. 3 different classification criteria and discuss the chemical composition of HQ Car and DD Vel in Sect. 4.

2. Data

The HQ Car spectra have been obtained with different instruments: one spectrum was taken with the echelle spectrograph on the 4m Blanco telescope at Cerro Tololo Inter-American Observatory (CTIO). It has a resolution of 28 000 and covers the

5500–8000 Å wavelength range with a S/N (per pixel) of 57 in the order containing H α . Another spectrum was obtained using the 2.2m ESO/MPG telescope and the FEROS echelle spectrograph at the ESO La Silla observatory (Kaufer et al. 1999). The spectrum covers the 3500–9200 Å wavelength range with a resolution of 48 000 and a S/N (per pixel) in excess of 150 over the largest part of the spectrum. Finally, two spectra were obtained with the HARPS (Mayor et al. 2003) echelle spectrograph mounted at the 3.6m telescope at the ESO La Silla observatory, which provides a resolution $R=115\,000$ over a wide spectral range (3800–6900 Å). They both reach a S/N of 50 at 650 nm.

We analysed two spectra for DD Vel: the first one consists of four back-to-back FEROS spectra¹ coadded in order to increase the S/N. The second² was obtained with the UVES (Dekker et al. 2000) echelle spectrograph ($R=40\,000$) using the DIC2 (437+760) configuration. The blue and red arms cover the wavelength intervals [3750–5000] Å and [5650–7600/7660–9460] Å. Relevant information concerning the observations and pulsation parameters of the Cepheids are listed in Table 1. As shown in the next sections, strong emission features become prominent at some phases, and the spectra are therefore not suitable for an accurate abundance determination. We used the CTIO spectrum ($\phi=0.361$) for HQ Car and the FEROS spectrum ($\phi\approx0.292$) in the case of DD Vel.

3. Classification

3.1. Classification based on the location on a colour-magnitude diagram

Following the suggestion of an anonymous referee, we performed a detailed comparison in the K_s-J-K colour-magnitude diagram to constrain the nature of the candidate Type II Cepheids. Figure 1 shows evolutionary prescriptions for α -enhanced horizontal branch (HB) evolutionary models (Pietrinferni et al. 2004, 2006) at fixed chemical composition (see labelled values) and the two targets. It shows the Zero-Age-Horizontal-Branch (ZAHB) and HB evolutionary models for three different values of the stellar masses ranging from 0.49 to 0.58 M_{\odot} . The apparent NIR magnitudes of the targets are based on 2MASS photometry (Skrutskie et al. 2006). They were unreddened using the empirical reddening law provided by Cardelli et al. (1989). The true distance modulus was estimated using the K-band period-luminosity relation for Type II Cepheids provided by Matsunaga et al. (2006). We found $M_K = -3.81$ mag for DD Vel and $M_K = -3.87$ mag for HQ Car. Data plotted in this figure show that the position of the targets agrees quite well, within the errors, with the current evolutionary prescriptions, thus further supporting the working hypothesis that they are Type II Cepheids. It also displays the instability strip for RR Lyrae and BL Herculis stars. The hottest edge shows the first overtone blue edge, while the coolest shows the fundamental red edge. Current pulsation predictions (Marconi et al., 2015, ApJ, submitted) suggest that the edges of the instability strip are independent of the metal content in the NIR bands. The above edges should be cautiously treated, since they have been slightly extrapolated to higher luminosities to cover the magnitude range of the targets.

¹ prog. ID: 060.A-9120

² prog. ID: 082.D-0901

Table 1: Spectroscopic observations of HQ Car and DD Vel.

Star	RA dms	Dec dms	V mag	Epoch d	Period d	JD d	Phase	Spectrograph
HQ Car	10 20 32.00	-61 14 57.4	11.84	2452784.603 ^a	14.06378 ^a	2450834.86370	0.361	CTIO ^c
						2455284.65800	0.766	FEROS
						2456411.53798	0.891	HARPS
						2456412.51417	0.961	HARPS
DD Vel	09 12 09.63	-50 22 33.6	12.18	2434746.312 ^b	13.1948 ^b	2454186.09017	0.291	FEROS ^d
						2454186.11160	0.292	FEROS ^d
						2454186.13302	0.294	FEROS ^d
						2454186.15443	0.296	FEROS ^d
						2454773.35198	0.798	UVES

Notes. ^(a) Computed from ASAS photometry ^(b) GCVS values ^(c) Spectrum used to derive the chemical composition of HQ Car ^(d) Spectra coadded and used to derive the chemical composition of DD Vel

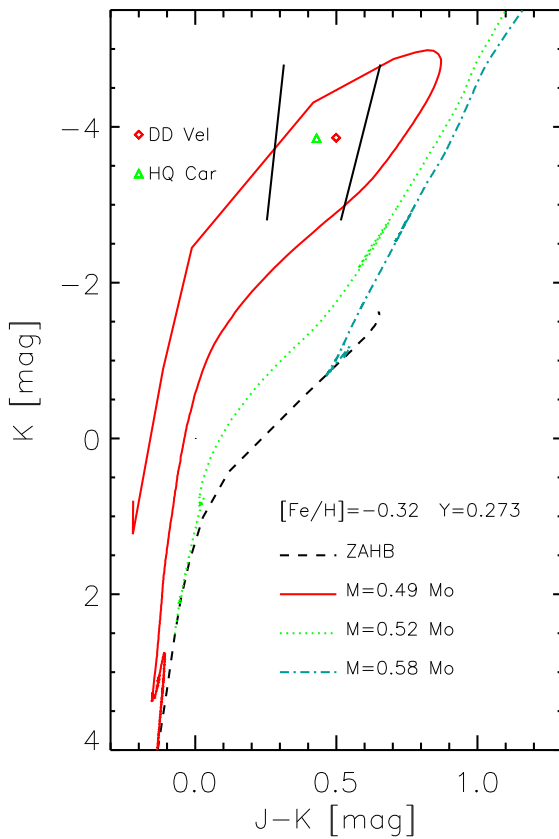


Fig. 1: Location of DD Vel and HQ Car in a K,J-K colour-magnitude diagram. The dashed line shows the zero-age-horizonal-branch (ZAHB), while the coloured lines display HB evolutionary models for stellar masses ranging from 0.49 to 0.58 M_{\odot} . The black lines display the instability strip for RR Lyrae and BL Herculis stars.

3.2. Classification based on emission features in the spectrum

3.2.1. Emission in $H\alpha$

The presence of emission in the $H\alpha$ lines of W Vir was first reported by Joy (1937) and Sanford (1953). Joy (1949)

noted that hydrogen line emission was a common feature of Type II Cepheids in globular clusters; it has afterwards also been reported in field Type II Cepheids (e.g., Wallerstein 1958; Harris & Wallerstein 1984). Following Schwarzschild (1953), the doubled absorption profiles, together with emission with an inverse P-Cygni profile in $H\alpha$, were early modeled as a shock-wave passing through the atmosphere in the rising part of the lightcurve (Whitney 1956a,b; Wallerstein 1959; Whitney & Scalafuris 1963): emission originates in the de-excitation region behind the radiative shock wave. Lèbre & Gillet (1992) used high resolution spectroscopy to follow the evolution of the emission profile of $H\alpha$ through an entire cycle of W Vir and further improved the shock model. Finally, Kovtyukh et al. (2011) extended this study to many metallic lines including Fe I, Fe II, Na I, and Ba II and concluded that W Vir consists in its inner part of a pulsating star with periodic shocks reaching the upper atmosphere and in its outer part of a circumstellar envelope.

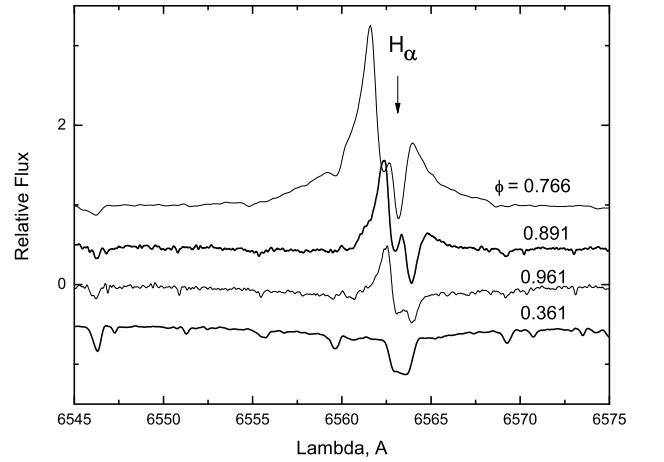


Fig. 2: Behaviour of the $H\alpha$ line in HQ Car at different phases.

In Fig. 2, we present the variations in the $H\alpha$ profile for HQ Car at four different phases. They are very similar to those presented for W Vir by Lèbre & Gillet (1992, their Fig. 3) and by Kovtyukh et al. (2011, their Fig. 12). The shock wave rising in the atmosphere of the star causes a broad emission feature comprising five components (3 in emission, 2 in absorption). The absorption features are associated to the presence of a circumstellar envelope for one and to the fall back of the upper atmo-

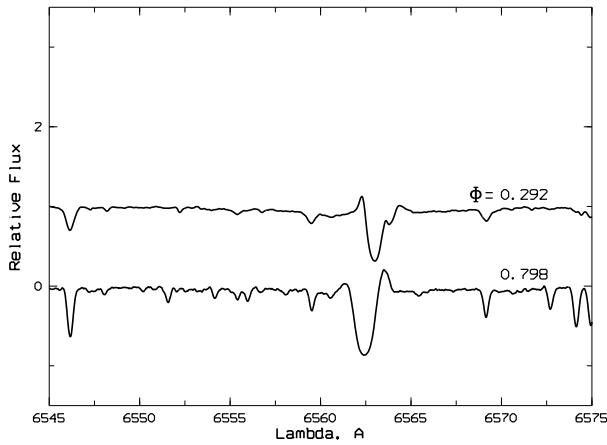


Fig. 3: Behaviour of the H α line in DD Vel at different phases.

sphere located above the shock for the other. In particular, the H α emission totally disappears at $\phi=0.361$, in good agreement with Lèbre & Gillet (1992), who mention that the shock emission is present during the entire cycle except between phases $\phi=0.38$ – 0.44 . In the case of DD Vel (Fig 3), the H α emission is weak as expected for $\phi=0.292$ but, more surprisingly, also weak at $\phi=0.798$. Given our limited phase coverage for this star, it could also very well be that we missed the phase of strong H α emission.

3.2.2. Emission in He I at 5875.64 Å

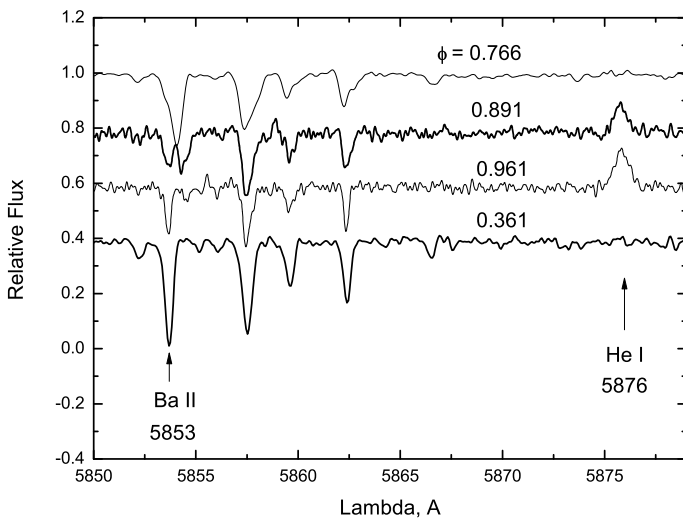


Fig. 4: Behaviour of the 5853 Ba II line and the 5876 He I line in HQ Car at different phases.

Emission lines of He I in the spectra of type II Cepheids were first mentioned by Wallerstein (1959). They enabled him to confirm the shock model. (The emission is caused by helium ionized by the shock wave that captures electrons.) More recent observations by Raga et al. (1989) were used to determine the H/He ratio in the atmosphere of W Vir. He I emission lines were extensively studied by both Lèbre & Gillet (1992) and Kovtyukh et al. (2011). The former reported the presence of emission in the He 5875.64 Å line between phases $\phi=0.827$ and $\phi=0.009$, while the latter detected emission between $\phi=0.865$

and $\phi=0.201$ for the same line. In both studies the emission peaks between $\phi\sim 0.8$ and $\phi\sim 0.1$, when the shock reaches its highest intensity.

In Fig. 4, we present the variations in the He I 5875.64 Å line profile for HQ Car at four different phases. Once again, they are very similar to those presented for W Vir by Lèbre & Gillet (1992, their Fig. 6) and by Kovtyukh et al. (2011, their Figs. 4,8). Emission is present only at the end of the cycle, at phases $\phi=0.891$ and $\phi=0.961$, in good agreement with previous studies. In the same figure, we note the doubling of the Ba II line profile in the same phases. The mechanism responsible for the line doubling was first explained by Schwarzschild (1953): line doubling can be observed when the shock wave moves across the layer of formation of a given absorption line, provided that this layer is thick enough; the blueshifted line is produced by cooling gas moving upwards, while the redshifted line originates in gas already falling down. In the case of DD Vel, Fig. 5 shows no emission for the He I 5875.64 Å line, but the Ba II line is split into two components at $\phi=0.798$, indicating that the region where the Ba II line is formed is crossed by the shock wave.

3.3. Kinematics consistent with a thick disc membership

Kinematics alone is not sufficient to decide that a star belongs to the thin or the thick disc. It is, however, interesting to investigate the kinematic properties of DD Vel and HQ Car. Therefore we computed their space velocities U_{LSR} , V_{LSR} , W_{LSR} in the local standard of rest³ using proper motions from the Naval Observatory Merged Astrometric Dataset (NOMAD, Zacharias et al. 2004) and the data shown in Table 2. Both stars have a total velocity $70 \leq v_{tot} \leq 180$ km/s, making them likely thick disc members (e.g., Nissen 2004). Their velocity along the direction of Galactic rotation V_{LSR} almost falls within -100 km/s and -40 km/s, the range quoted by Reddy et al. (2003) for a probable thick-disc membership. Finally, comparing the stars in our sample to the velocity–metallicity plots of Bensby et al. (2007, see their Fig. 1), we find that U_{LSR} is not conclusive for HQ Car, while V_{LSR} and W_{LSR} both place this star in the thick disc. The situation is a bit less clear for DD Vel because its U_{LSR} is still at the upper limit for a thin disc star, and its V_{LSR} at the lower

³ $[U_{\odot}, V_{\odot}, W_{\odot}] = [11.10, 12.24, 7.25]$ km/s (Schönrich et al. 2010)

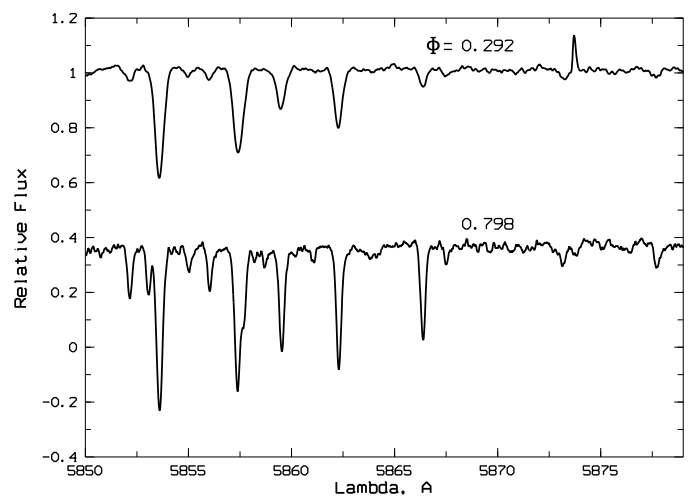


Fig. 5: Same as Fig. 4 for DD Vel.

limit, whereas its W_{LSR} is typical of the thick disc. In conclusion, HQ Car seems to be a very likely thick-disc member, whereas it cannot be totally excluded that DD Vel is a thin-disc member. The above kinematical evidence therefore supports the hypothesis that both stars are Type II Cepheids in the thick disc rather than classical Cepheids located in the thin disc.

3.4. Classification based on the chemical composition

From their period (with respect to the classification of Soszyński et al. (2008b) for Type II Cepheids) and the emission features in H α and He I at 5876 Å, it already appears to be clear that both HQ Car and DD Vel are W Vir stars. This will be reinforced in Sect. 4 where we examine their chemical composition.

4. Chemical composition

4.1. Method

We used the DECH 30 software package⁴ to normalize the individual spectra to the local continuum, to identify the lines of different chemical elements, and to measure the equivalent widths (EW) of the absorption lines. The oscillator strengths have been taken from the Vienna Atomic Lines Database (VALD Kupka et al. 1999).

To determine the effective temperature T_{eff} , we employed the line depth ratios method of Kovtyukh (2007), which comes from the work of Kovtyukh & Gorlova (2000). The ratios of the central depths of carefully chosen pairs of lines that have a very different dependence on T_{eff} are entered in previously calibrated relations. This technique allows determining T_{eff} with great precision: the use of several tens (≥ 50) of ratios per spectrum leads to uncertainties of ≈ 10 -20 K when $S/N > 100$ and of ≈ 30 -50 K when $S/N < 100$. The method is independent of the interstellar reddening and only marginally dependent on the individual characteristics of stars, such as rotation, microturbulence, and metallicity.

To determine the surface gravity ($\log g$) and the microturbulent velocity V_t , we used a canonical analysis. We sought the surface gravity from the excitation equilibrium of Fe I and Fe II lines, and the microturbulent velocity is determined from the Fe I lines. We note that the excitation equilibrium is also satisfied by V I and V II and, to a slightly lesser extent, by Ti I and Ti II in HQ Car, while it is satisfied for the couples Si I / Si II, Ti I / Ti II (but not Cr I / Cr II) in the case of DD Vel. As far as the microturbulent velocity is concerned, an innovative approach using lines of several elements has been developed by Sahin et al. (2011) and is illustrated in Reddy et al. (2012). In this method, the standard errors are plotted as a function of the microturbulent velocity. We applied it to the stars in our sample, and the results are in good agreement with our values for V_t . They are described in Appendix A. The atmospheric parameters for DD Vel and HQ Car are listed in Table 3.

Table 3: Atmospheric parameters derived for HQ Car and DD Vel.

Star	T_{eff} K	$\log g$ dex	V_t km/s	[Fe/H] dex
HQ Car	5580	1.6	3.1	-0.32
DD Vel	5572	1.4	3.8	-0.48

⁴ <http://www.gazinur.com/DECH-software.html>

Table 4: Individual abundances [X/H] in HQ Car and DD Vel.

		HQ Car			DD Vel		
Ion		[X/H]	σ	N	[X/H]	σ	N
C I	6.00	-0.14	0.19	7	-0.48	0.15	2
N I	7.00	0.20	0.21	2	0.23	0.11	2
O I	8.00	0.23	0.01	2	-0.22		1
Na I	11.00	-0.25	0.09	3	-0.33	0.12	4
Mg I	12.00	-0.17		1	-0.41		1
Al I	13.00	-0.43	0.18	4			
Si I	14.00	-0.11	0.12	22	-0.24	0.14	20
Si II	14.01				-0.28	0.15	2
S I	16.00	-0.05	0.12	5	-0.39	0.00	2
Ca I	20.00	-0.47	0.18	9	-0.73	0.06	14
Sc II	21.01	-0.55 [†]			-1.12 [†]		
Ti I	22.00	-0.35	0.19	6	-0.61	0.11	13
Ti II	22.01	-0.28		1	-0.61	0.11	4
V I	23.00	-0.39	0.13	9	-0.48	0.10	4
V II	23.01	-0.43	0.13	2			
Cr I	24.00	-0.59	0.23	3	-0.85	0.06	7
Cr II	24.01				-0.51	0.10	7
Mn I	25.00	-0.63 [†]			-0.71 [†]		
Fe I	26.00	-0.32	0.10	133	-0.48	0.11	162
Fe II	26.01	-0.32	0.07	8	-0.51	0.09	19
Co I	27.00	-0.18	0.19	5	-0.38	0.17	3
Ni I	28.00	-0.34	0.13	38	-0.52	0.06	44
Cu I	29.00	-0.48 [†]			-0.43 [†]		
Zn I	30.00				-0.20	0.05	2
Y II	39.01	-0.82	0.10	2	-1.41	0.13	3
Zr II	40.01	-1.16		1			
La II	57.01	-0.72	0.08	3			
Nd II	60.01	-0.58		1	-0.89	0.07	2
Eu II	63.01	-0.04		1			

Notes. ^(†) Abundance determined by spectral synthesis

The lines of odd-Z elements can be broadened due to their hyperfine structure (hfs). However, the hfs corrections are negligible in the case of V or Co for the considered EW. This is not true in the case of Sc, Mn, or Cu (e.g., North et al. 2012; Reddy et al. 2012). We therefore computed the abundances of these elements via spectral synthesis using the 5526.79, 5657.90, 5667.15, 6245.62, 6604.60 lines for Sc II, 5420.35, 5432.56, 6013.48, 6021.79 for Mn I and 5105.55, 5218.21, 5782.14 for Cu I, and the STARSP code developed by Tsymbal (1996). We took the hyperfine structure of Sc II (Prochaska & McWilliam 2000), Mn I, and Cu I (Allen & Porto de Mello 2011) into account for the line profile calculations.

Atmospheric models are interpolated for each Type II Cepheid using the grid of 1D, LTE atmosphere models of Castelli & Kurucz (2004). Individual abundances are listed in Table 4 and abundance ratios (with respect to iron) in Table 5. We computed the solar reference abundances using lines in the Sun with EWs < 120 mÅ and the same atmosphere models (Castelli & Kurucz 2004). They are listed in the Appendix B, together with the prescriptions of Asplund et al. (2009) and the solar abundances of Reddy et al. (2003) that are used by Reddy et al. (2006) in their study of the thick disc.

We used 25 calibrations to determine the effective temperature of HQ Car and 26 calibrations for DD Vel, leading to standard deviations of 95 K and 109 K, respectively, and standard errors of 19 K and 22 K. We adopted 100 K as the uncertainty on T_{eff} . We estimated the uncertainty on $\log g$ as ± 0.2 dex and the uncertainty on V_t as ± 0.5 km/s. Table 6 lists the variations

Table 2: Kinematics of HQ Car and DD Vel.

Star	RA deg	Dec deg	PM (RA) mas/yr	PM (Dec) mas/yr	Vrad km/s	Distance pc	U_{LSR} km/s	V_{LSR} km/s	W_{LSR} km/s	v_{LSR}^e km/s
HQ Car	155.133	-61.249	1.1±2.6 ^a	2.9±2.6 ^a	62.05 ^b	5725 ^d	10.13	-57.07	85.55	103.34
DD Vel	138.040	-50.376	-5.7±4.7 ^a	-1.3±4.7 ^a	26.02 ^c	2444 ^d	44.78	-33.23	-51.75	76.08

Notes. ^(a) NOMAD catalogue (Zacharias et al. 2004). ^(b) Radial velocity measured in our CTIO spectrum. The other spectra show line doubling with radial velocities of 85.26 & 108.7 km/s (FEROS), 79.78 & 113.8 km/s, 74.68 & 120.0 km/s (HARPS), respectively. ^(c) γ -velocity of DD Vel from Metzger et al. (1992). ^(d) Distance derived from the apparent magnitude in the J band (2MASS) and the period-luminosity relation of Matsunaga et al. (2006). ^(e) $v_{LSR} = (U_{LSR}^2 + V_{LSR}^2 + W_{LSR}^2)^{1/2}$

Table 5: Abundance ratios [X/Fe] in HQ Car and DD Vel.

		HQ Car				DD Vel	
Ion		[X/Fe]	σ	[X/Fe] ^I	σ^I		
C I	6.00	+0.18	0.21			+0.00	0.19
N I	7.00	+0.52	0.23			+0.71	0.16
O I	8.00	+0.55	0.10			+0.26	0.11
Na I	11.00	+0.07	0.13			+0.15	0.16
Mg I	12.00	+0.15	0.10			+0.07	0.11
Al I	13.00	−0.11	0.21				
Si I	14.00	+0.21	0.16	+0.44	0.18	+0.24	0.18
Si II	14.01					+0.20	0.19
S I	16.00	+0.27	0.16			+0.09	0.11
Ca I	20.00	−0.15	0.21	−0.04	0.22	−0.25	0.13
Sc II	21.01	−0.23	0.10			−0.64	0.11
Ti I	22.00	−0.03	0.21	−0.01		−0.13	0.16
Ti II	22.01	+0.04	0.10	−0.07		−0.13	0.16
V I	23.00	−0.07	0.16			+0.00	0.15
V II	23.01	−0.11	0.16				
Cr I	24.00	−0.27	0.25			−0.37	0.13
Cr II	24.01					−0.03	0.15
Mn I	25.00	−0.31	0.10			−0.23	0.11
Co I	27.00	+0.14	0.21			+0.10	0.20
Ni I	28.00	−0.02	0.16			−0.04	0.13
Cu I	29.00	−0.16	0.10			+0.05	0.11
Zn I	30.00					+0.28	0.12
Y II	39.01	−0.50	0.14			−0.93	0.17
Zr II	40.01	−0.84	0.10				
La II	57.01	−0.40	0.13				
Nd II	60.01	−0.26	0.10			−0.41	0.13
Eu II	63.01	+0.28	0.10	+0.06			

Notes. ⁽¹⁾ Yong et al. (2006)

in the individual abundances [X/H] when changing the atmospheric parameters by $\Delta T_{\text{eff}} = +100$ K, $\Delta \log g = +0.2$ dex, and $\Delta V_t = +0.2$ km/s and their sum in quadrature, which we adopt as the uncertainty on the abundances due to the uncertainties on the atmospheric parameters. It is well documented (e.g., Johnson 2002) that such a method leads to overestimated values for the total error, because by construction it ignores covariances between the different atmospheric parameters. They nevertheless remain lower than 0.10 dex in most cases. The sum in quadrature of the errors associated with the uncertainties on the atmospheric parameters and of the standard deviation associated with the determination of the abundance of a given element gives the total error on the abundance for this element.

4.2. Chemical composition

The two stars in our sample have [Fe/H] in the -0.3 to -0.5 dex range, towards the lower end of the metallicity distribution

Table 6: Abundance uncertainties due to uncertainties on the atmospheric parameters, computed for HQ Car ($T_{\text{eff}} = 5580$ K, $\log g = 1.6$ dex, $V_t = 3.1$ km/s, [Fe/H] = -0.327 dex). Cols. 3–5 are the errors associated with the uncertainties on one of the individual atmospheric parameters. Col. 6 is the total error associated with the uncertainties on the atmospheric parameters. Col. 7 is the total error, adding in quadrature col. 6 and the standard deviations listed in Table 4 for individual species.

Ion		ΔT_{eff} +100 K	$\Delta \log g$ +0.2 dex	ΔV_t +0.5 km/s	Total (atm)	Total
C I	6.00	-0.06	0.08	-0.02	0.10	0.21
N I	7.00	-0.09	0.08	-0.02	0.12	0.24
O I	8.00	0.05	0.08	-0.03	0.10	0.10
Na I	11.00	0.05	0.00	-0.04	0.06	0.11
Mg I	12.00	0.05	0.00	-0.07	0.09	0.09
Al I	13.00	0.03	-0.01	-0.01	0.03	0.18
Si I	14.00	0.04	0.00	-0.03	0.05	0.13
Si II	14.01	-0.07	0.09	-0.12	0.17	0.17
S I	16.00	-0.03	0.07	-0.03	0.08	0.14
Ca I	20.00	0.07	0.00	-0.09	0.11	0.21
Sc II	21.01	0.03	0.08	-0.08	0.12	0.12
Ti I	22.00	0.09	0.00	-0.02	0.09	0.21
Ti II	22.01	0.02	0.07	-0.04	0.08	0.08
V I	23.00	0.10	-0.01	-0.01	0.10	0.16
V II	23.01	0.01	0.07	-0.02	0.07	0.15
Cr I	24.00	0.05	-0.01	-0.01	0.05	0.24
Mn I	25.00	0.07	-0.01	-0.05	0.09	0.09
Fe I	26.00	0.07	-0.01	-0.05	0.09	0.13
Fe II	26.01	-0.01	0.08	-0.04	0.09	0.11
Co I	27.00	0.11	-0.01	-0.01	0.11	0.22
Ni I	28.00	0.07	-0.01	-0.04	0.08	0.15
Cu I	29.00	0.10	-0.01	-0.03	0.10	0.10
Y II	39.01	0.02	0.07	-0.01	0.07	0.12
Zr II	40.01	0.02	0.07	-0.01	0.07	0.07
La II	57.01	0.05	0.07	-0.01	0.09	0.12
Nd II	60.01	0.05	0.07	0.00	0.09	0.09
Eu II	63.01	0.04	0.08	-0.04	0.10	0.10

for BL Her stars, but still in a domain where the metallicities of BL Her and W Vir stars overlap (see Maas et al. 2007). As shown just after this, they are probably affected by dust-gas separation. However, the [S/Fe] we measured for DD Vel (+0.09 dex) and HQ Car (+0.27 dex) are very similar to those already reported for [S/Fe] in different Galactic structures. Below [Fe/H] = -1.0 dex, [S/Fe], values are scattered around a plateau at $\approx +0.25$ dex and decrease at higher metallicities until reaching [S/Fe] = 0.0 dex at [Fe/H] = -0.3 dex (e.g., François 1987, 1988; Chen et al. 2002; Nissen et al. 2007; Matrozis et al. 2013; Caffau et al. 2014, and references therein). Also our [Zn/Fe] measurement of $+0.28 \pm 0.12$ dex in DD Vel is very consistent with previous values ([Zn/Fe] $\approx +0.1$ – $+0.2$ dex) reported for the thick disc (e.g., Mishenina et al. 2002; Bensby et al. 2005;

Brewer & Carney 2006; Reddy et al. 2006). Since sulphur and zinc are only slightly depleted into dust (Savage & Sembach 1996), the typical thick-disc values for $[S/Fe]$ and $[Zn/Fe]$ in HQ Car and DD Vel indicate that their iron abundances are probably not very modified by the dust-gas separation. In particular, this allows us to use an average thick disc star for the -0.45 to -0.55 dex $[Fe/H]$ bin for comparison purposes (Reddy et al. 2006, col. 4 in their Table 7).

Maas et al. (2007) have shown that W Vir stars have $[Na/Fe]$ that is independent of $[Fe/H]$ and consistent with thick disc stars where $\langle[Na/Fe]\rangle = +0.12$ dex (Reddy et al. 2006). This argument does not apply to the stars with a severe dust-gas separation. They find, in contrast, that BL Her stars are strongly overabundant in sodium with a mean $[Na/Fe] = +0.73$ dex. For the two Type II Cepheids in our sample, $[Na/Fe]$ varies between $+0.07$ and $+0.15$ dex, similar to the representative thick disc value (see Fig. 6). Since iron could be affected by dust-gas separation, we also compare $[Na/Zn]$ for the BL Her and W Vir stars, and again DD Vel has low $[Na/Zn]$ similar to the other W Vir stars, while the BL Her stars show very high ($>+0.5$ dex) values of $[Na/Zn]$. The absence of Na overabundance in our sample confirms that they are W Vir stars and not BL Her stars, as could already be inferred from their period ($P > 4d$).

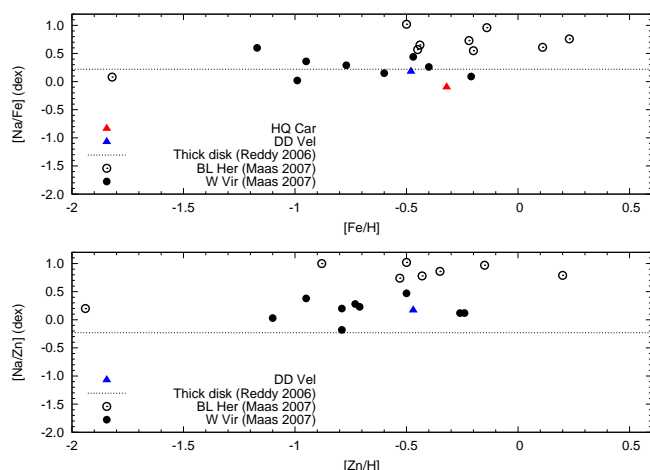


Fig. 6: *Top*: $[Na/Fe]$ vs. $[Fe/H]$ for BL Her stars (open circles) and W Vir stars (filled circles) from Maas et al. (2007). HQ Car and DD Vel are overplotted in red and blue, respectively. The ratio for a representative thick-disc star at $[Fe/H] = -0.5$ dex is shown as a dashed line. *Bottom*: same for $[Na/Zn]$ vs. $[Zn/H]$. Abundances have been rescaled to the solar abundances of Reddy et al. (2003), used as a reference by Maas et al. (2007).

When gas cools sufficiently, dust grains can form and the abundances of the elements in the gas phase decrease. Because this happens at different temperatures for different trace elements, the quantity "50% condensation temperature" ($50\% T_c$) has been defined, at which 50% of the element is found in the gas phase and the other 50% is locked in dust grains. We adopted the $50\% T_c$ determined by Lodders (2003). A correlation between the underabundance of a given element and its condensation temperature is then interpreted as a dust-gas separation⁵.

⁵ It should be noted that this assumption involves implicit approximations (such as the formation of dust grains under conditions of thermo-

As can be seen in Fig. 7, the Type II Cepheids in our sample show hints of (mild) dust-gas separation: the more volatile elements have abundances similar to those of an average thick-disc star (Reddy et al. 2006), while the refractory elements are underabundant, because they are depleted into dust. For a better visibility, we focus in Fig. 8 on the elements with $50\% T_c > 1300$ K.

As expected, the signature of dust-gas separation is especially marked for the elements with the highest $50\% T_c$. In HQ Car, Ca, Nd, Al, and Sc are mildly depleted by ~ -0.2 dex and Y by ~ -0.3 dex with respect to an average thick-disc star. Zr seems to be very depleted because $[Zr/H]$ clearly falls below the abundances of the other neutron-capture elements, but we have no comparison with an average thick-disc star to draw a firm conclusion. The depletion is more severe for DD Vel as the underabundances with respect to an average thick disc star reach ~ -0.30 dex for Ti, ~ -0.45 dex for Nd and Ca, ~ -0.80 dex for Sc and ~ -0.90 dex for Y. To further support the dust-gas separation, we note that most of the individual abundances fall below those of the thick-disc reference star for the elements with $50\% T_c > 1400$ K.

Hints or even clear evidence of dust-gas separation in Type II Cepheids have already been reported for ST Pup by Gonzalez & Wallerstein (1996) and for CO Pup, V1711 Sgr, MZ Cyg, and SZ Mon by Maas et al. (2007). On the other hand, these authors find the signature of dust-gas separation less convincing in RX Lib and W Vir because it relies mostly on the depletion in Sc. As we discuss in more detail in the next paragraph, severe dust-gas separation has also been reported in most of the RV Tau stars (see Giridhar et al. 2005, and references therein). Maas et al. (2007) found a Type II Cepheid (CC Lyr) with an extreme dust-gas separation, which is larger than in any RV Tau star. It is important to note that all the Type II Cepheids with a signature of dust-gas separation are W Vir stars and not BL Her stars. That the stars in our sample also show possible (HQ Car) or probable (DD Vel) signs of this phenomenon reinforces their classification as W Vir stars.

Dust-gas separation is a common feature in RV Tau stars (see Giridhar et al. 2005, and references therein). In a qualitative scenario (Waters et al. 1992), binary RV Tau stars are surrounded by a dusty disc. The dust-gas separation occurs when radiation pressure traps the dust grains in the disc while some of the gas (deprived from dust) is re-accreted on the star via the viscous disc that allows for transfer of angular momentum. The origin of the circumbinary disc in RV Tau stars is not clear, but it is generally believed to be created during binary interaction when the primary was a giant.

This scenario excludes metal-poor systems ($[Fe/H] \leq -1.0$ dex) where dust cannot form in sufficient quantities, and indeed no sign of dust-gas separation has been found for metal-poor RV Tau variables in globular clusters (Gonzalez & Lambert 1996). Similarly, Maas et al. (2007) find no evidence of dust-gas separation for TW Cap, a W Vir star with $[Fe/H] = -1.8$ dex possibly associated to the halo of the Milky Way.

It is not clear that the dust-gas separation has the same origin in W Vir stars as in RV Tau stars. In particular, the observed depletion is generally much shallower in the W Vir stars. Only in the case of CC Lyr does it reach the extreme values more commonly seen in RV Tau stars (e.g., ~ -3.0 dex in HP Lyr and

dynamic equilibrium) that may not be met in the surroundings of W Vir stars due to the presence of shocks in the atmosphere (Kovtyukh et al. 2011).

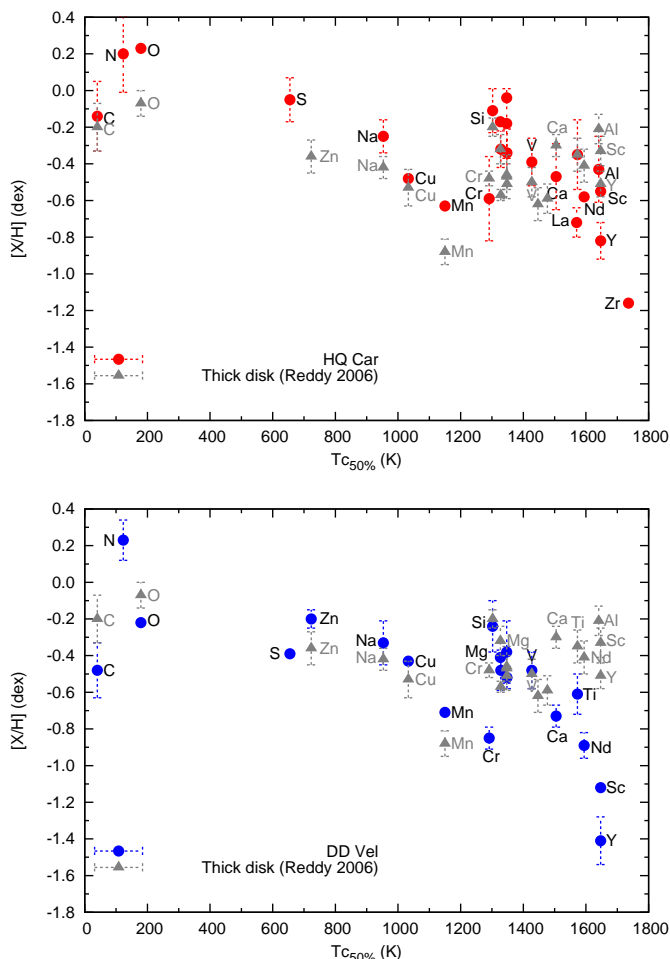


Fig. 7: $[X/H]$ vs. 50% T_c for the two Type II Cepheids in our sample. An average thick-disc star (grey dots) is plotted for comparison. Elements are identified by their chemical symbol. Abundances have been rescaled to the solar abundances that we recomputed with the Castelli & Kurucz (2004) models (See Appendix B)

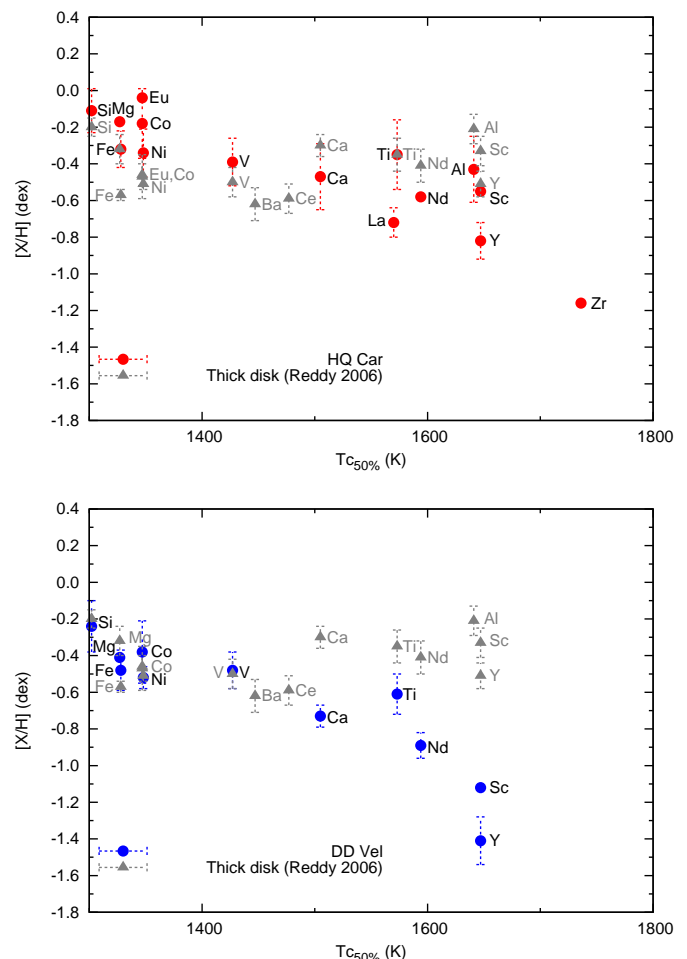


Fig. 8: Same as Fig. 7, but focusing on the elements with the highest condensation temperature.

DY Ori, see Giridhar et al. 2005). The RV Tau stars depleted in their refractory elements are known binaries for a large number of them, supporting the hypothesis of a circumbinary dusty disc (Rao et al. 2012). Disentangling orbital velocities from pulsational velocities is very demanding in terms of observing time both in the case of RV Tau and W Vir stars, and indeed only four type II Cepheids are currently known as binaries: AU Peg, IX Cas, TX Del, and ST Pup. It is interesting to note that the only W Vir star in this group (ST Pup) shows obvious signs of dust-gas depletion, while the other shorter-period stars do not.

Recently reported observational (e.g., Marengo et al. 2010b) and theoretical (e.g., Neilson et al. 2012) lines of evidence support the existence of mass loss in classical Cepheids; however, these outflows seem to have a very low dust content (Marengo et al. 2013), possibly indicating that the wind is driven by pulsation and is not dust-driven as generally observed in evolved stars. On the other hand, extended dusty environments have been detected with high angular resolution techniques (e.g., Kervella et al. 2006; Gallenne et al. 2013, and references therein) and from extended emission in the mid- and far-infrared

(Barmby et al. 2011). They have been attributed to the presence of a circumstellar envelope around the Cepheids.

As far as Type II Cepheids are concerned, Kovtyukh et al. (2011) analysed hydrogen, helium, and metallic lines in W Vir itself. They were able to reproduce the specifics of spectral line variability in W Vir with the help of a non-linear pulsation model. Results suggest that W Vir consists of two different layers, the inner part being the pulsating star itself and the outer part a very extended and dense atmosphere, and it might even include a circumstellar envelope with a very low expansion rate.

If the most desirable experiment in the near future were to systematically examine the binarity properties of W Vir stars, it would nevertheless be interesting to investigate whether dust-gas separation could also somehow take place in their circumstellar envelopes.

5. Summary and conclusion.

The status of the HQ Car and DD Vel Type II Cepheids has remained unclear. Depending on the catalogue (i.e., on the method and criteria used to perform the classification), they are sometimes listed as classical Cepheids and sometimes as Type II.

Because we observed emission features in the $H\alpha$ and in the 5875.64 Å He I lines that are characteristic features of W Vir stars, we conclude that HQ Car and DD Vel are Type II Cepheids from this sub-class. Their periods of 14.06 and 13.19 days, respectively, and the absence of Na overabundance further indicates that they are not BL Her stars. Moreover, they show a possible (HQ Car) or probable (DD Vel) signature of mild dust-gas separation. Such abundance patterns have currently been observed only in long-period Type II Cepheids and RV Tau stars, thus reinforcing our classification.

Several studies of the Galactic abundance gradients in the thin disc using classical Cepheids have reported increased dispersion in the outer disc (Yong et al. 2006; Lemasle et al. 2008; Luck et al. 2011; Luck & Lambert 2011; Genovali et al. 2014); however, these findings are hampered by the possible contamination of the current samples by misclassified Type II Cepheids that are thick-disc members. Including unrecognized Type II Cepheids modifies the abundance patterns not only because they belong to another stellar population but also because their current distances are computed with period-luminosity relations that are only valid for classical Cepheids. Thick-disc members can be identified by their specific location in the $[\alpha/\text{Fe}]$ vs $[\text{Fe}/\text{H}]$ plane (e.g., Recio-Blanco et al. 2014), and recent studies indicate that the thin disc contamination by thick-disc stars is not negligible (see, for instance, Mikolaitis et al. 2014, their Fig. 7).

Acknowledgements. The authors thank the anonymous referees for the very valuable comments that helped to improve the quality of this paper. The authors thank Dr. D. Yong and Prof. B.W. Carney for providing the HQ Car spectrum. The authors thank Profs. C. Dominik and L.B.F.M. Waters for useful discussions on the dust-gas separation phenomenon. V.K. acknowledges the support from the Swiss National Science Foundation, project SCOPES No. IZ73Z0152485. GG acknowledges the support of the Chilean fund FONDECYT-regular (project 1120190).

References

- Allen, D. M., Porto de Mello, G. F., 2011, *A&A* 525, 63
- Anderson, K. S., Kraft, R. P., 1971, *ApJ* 167, 119
- Andrievsky, S. M., Kovtyukh, V. V., Luck, R. E., Lépine, J. R. D., Bersier, D., Maciel, W. J., Barbuy, B., Klochkova, V. G., Panchuk, V. E., Karpischek, R. U., 2002, *A&A* 381, 32
- Asplund, M., Grevesse, N., Sauval, A. J., Scott, P., 2009, *ARA&A* 47, 481
- Barker, T., Baumgart, L. D., Butler, D., Cudworth, K. M., Kemper, E., Kraft, R. P., Lorre, J., Kameswara Rao, N., Reagan, G. H., Soderblom, D. R., 1971, *ApJ* 167, 119
- Barmby, P., Marengo, M., Evans, N. R., Bono, G., Huelsman, D., Su, K. Y. L., Welch, D. L., Fazio, G. G., 2011, *AJ* 141, 42
- Bensby, T., Feltzing, S., Lundström, I., Ilyin, I., 2005 *A&A* 433, 185
- Bensby, T., Zenn, A. R., Oey, M. S., Feltzing, S., 2007b, *ApJ* 663, L13
- Bono, G., Caputo, F., Santolamazza, P., 1997, *A&A* 317, 171
- Brewer, M. M., Carney, B. W., 2006, *AJ* 131, 431
- Caffau, E., Monaco, L., Spite, M., Bonifacio, P., Carraro, G., Ludwig, H.-G., Villanova, S., Beletsky, Y., Sbordone, L., 2014, *A&A* 568, A29
- Cardelli, J. A., Clayton, G. C., Mathis, J. S., 1989, *ApJ* 345, 245
- Castellani, V., Calamida, A., Bono, G., Stetson, P. B., Freyhammer, L. M., Degl'Innocenti, S., Prada Moroni, P., Monelli, M., Corsi, C. E., Nonino, M., Buonanno, R., Caputo, F., Castellani, M., Dall'Orta, M., Del Principe, M., Ferraro, I., Iannicola, G., Piersimoni, A. M., Pulone, L., Vuerli, C., 2007, *ApJ* 663, 1021
- Castelli F., Kurucz R. L., 2004, arXiv:astro-ph/0405087
- Chen, Y. Q., Nissen, P. E., Zhao, G., Asplund, M., 2002, *A&A*, 390, 225
- Dekker, H., D'Odorico, S., Kaufer, A., Delabre, B., Kotzłowski, H., 2000, *SPIE* 4008, 534
- Fernie, J.D., Beattie, B., Evans, N. R., Seager, S., 1995, *IBVS* No. 4148
- François, P., 1987, *A&A* 176, 294
- François, P., 1988, *A&A* 195, 226
- Gallenne, A., Mérand, A., Kervella, P., Chesneau, O., Breitfelder, J., Gieren, W., 2013, *A&A* 558, A140
- Genovali, K., Lemasle, B., Bono, G., Romaniello, M., Fabrizio, M., Ferraro, I., Iannicola, G., Laney, C. D., Nonino, M., Bergemann, M., Buonanno, R., François, P., Inno, L., Kudritzki, R.-P., Matsunaga, N., Pedicelli, S., Primas, F., Thévenin, F., 2014, *A&A* 566, A37
- Gingold, R. A., 1985, *MmSAI* 56, 169
- Giridhar, S., Lambert, D. L., Reddy, B. E., Gonzalez, G., Yong, D., 2005, *ApJ* 627, 432
- Gonzalez, G., Wallerstein, G., 1996, *MNRAS* 280, 515
- Gonzalez, G., Lambert, D. L., 1997, *AJ* 114, 341
- Harris, H. C., Wallerstein, G., 1984, *AJ* 89, 379
- Harris, H. C., 1985, *AJ* 90, 756
- Johnson, J. A. 2002, *ApJSS*, 139, 219
- Joy, A. H., 1937, *ApJ* 86, 363
- Joy, A. H., 1949, *ApJ* 110, 105
- Kaufer, A., Stahl, O., Tubbesing, S., Nørregaard, P., Avila, G., François, P., Pasquini, L., Pizzella, A., 1999, *Msngr* 95, 8
- Kervella, P., Mérand, A., Perrin, G., Coudé Du Foresto, V., 2006, *A&A* 448, 623
- Kovtyukh, V. V., Gorlova, N. I., 2000, *A&A* 358, 587
- Kovtyukh, V. V., 2007, *MNRAS* 378, 617update
- Kovtyukh, V. V., Wallerstein, G., Andrievsky, S. M., Gillet, D., Fokin, A. B., Templeton, M., Henden, A. A., 2011, *A&A* 526, A116
- Kupka, F., Piskunov, N. E., Ryabchikova, T. A., Stempels, H. C., Weiss W. W., 1999, *A&AS*, 138, 119
- Lèbre, A., Gillet, D., 1992, *A&A* 255, 221
- Lemasle, B., François, P., Piersimoni, A., Pedicelli, S., Bono, G., Laney, C. D., Primas, F., Romaniello, M., 2008, *A&A* 490, 613
- Lodders, K., 2003, *ApJ* 591, 1220
- Luck, R. E.; Andrievsky, S. M., Kovtyukh, V. V., Gieren, W., Graczyk, D., 2011, *AJ* 142, 51
- Luck, R. E., Lambert, D. L., 2011, *AJ* 142, 136
- Maas, T., Giridhar, S., Lambert, D. L., 2007, *ApJ* 666, 378
- Marengo, M., Evans, N. R., Barmby, P., Matthews, L. D., Bono, G., Welch, D. L., Romaniello, M., Huelsman, D., Su, K. Y. L., Fazio, G. G., 2010, *ApJ* 725, 2392
- Marengo, M., Evans, N. R., Matthews, L. D., Bono, G., Barmby, P., Welch, D. L., Romaniello, M., Su, K. Y. L., Fazio, G. G., Huelsman, D., 2013, *ASSP* 31, 99
- Matsunaga, N., Fukushi, H., Nakada, Y., Tanabé, T., Feast, M. W., Menzies, J. W., Ita, Y., Nishiyama, S., Baba, D., Naoi, T., Nakaya, H., Kawadu, T., Ishihara, A., Kato, D., 2006, *MNRAS* 370, 1979
- Mayor, M., Pepe, F., Queloz, D., Bouchy, F., Rupprecht, G., Lo Curto, G., Avila, G., Benz, W., Bertaux, J.-L., Bonfils, X., and 22 coauthors, 2003, *Msngr* 114, 20
- Matrozi, E., Ryde, N., Dupree, A. K., 2013, *A&A* 559, A115
- Metzger, M. R., Caldwell, J. A. R., Schechter, P. L., 1992, *AJ* 103, 529
- Mikolaitis, S., Hill, V., Recio-Blanco, A., de Laverny, P., Allende Prieto, C., Kordopatis, G., Tautvaisiene, G., Romano, D., Gilmore, G., Randich, S., Feltzing, S., Micela, G., Vallenari, A., Alfaro, E. J., Bensby, T., Bragaglia, A., Flaccomio, E., Lanzafame, A. C., Pancino, E., Smiljanic, R., Bergemann, M., Carraro, G., Costado, M. T., Damiani, F., Hourihane, A., Jofré, P., Lardo, C., Magrini, L., Maiorca, E., Morbidelli, L., Sbordone, L., Sousa, S. G., Worley, C. C., Zaggia, S., 2014, *A&A* 572, A33
- Mishenina, T. V., Kovtyukh, V. V., Soubiran, C., Travaglio, C., Busso, M., 2002, *A&A* 396, 189
- Neilson, H. R., Langer, N., Engle, S. G., Guinan, E., Izzard, R., 2012, *ApJ* 760, 18
- Nissen, P. E., 2004, in *Origin and Evolution of the Elements*, Carnegie Observatories Astrophysics Series, eds. A. McWilliam & M. Rauch, 4, 156
- Nissen, P. E., Akerman, C., Asplund, M., Fabbian, D., Kerber, F., Kaufl, H. U., Pettini, M., 2007, *A&A* 469, 319
- North, P., Cescutti, G., Jablonka, P., Hill, V., Shetrone, M., Letarte, B., Lemasle, B., Venn, K. A., Battaglia, G., Tolstoy, E., Irwin, M. J., Primas, F., François, P., 2012, *A&A* 541, 45
- Pietrinferni, A., Cassisi, S., Salaris, M., Castelli, F., 2004, *ApJ* 612, 168
- Pietrinferni, A., Cassisi, S., Salaris, M., Castelli, F., 2006, *ApJ* 642, 797
- Pojmanski, G., 2002, *AcA* 52, 397
- Prochaska, J. X., McWilliam, A., 2000, *ApJ* 537, 57
- Raga, A., Wallerstein, G., Oke, J. B., 1989, *ApJ* 347, 1107
- Rao, S. S., Giridhar, S., Lambert, D. L., 2012, *MNRAS* 419, 1254
- Recio-Blanco, A., de Laverny, P., Kordopatis, G., Helmi, A., Hill, V., Gilmore, G., Wyse, R., Adibekyan, V., Randich, S., Asplund, M., Feltzing, S., Jeffries, R., Micela, G., Vallenari, A., Alfaro, E., Allende Prieto, C., Bensby, T., Bragaglia, A., Flaccomio, E., Koposov, S. E., Korn, A., Lanzafame, A., Pancino, E., Smiljanic, R., Jackson, R., Lewis, J., Magrini, L., Morbidelli, L., Prisinzano, L., Sacco, G., Worley, C. C., Hourihane, A., Bergemann, M., Costado, M. T., Heiter, U., Jofré, P., Lardo, C., Lind, K., Maiorca, E., 2014, *A&A* 567, 5
- Reddy, B. E., Tomkin, J., Lambert, D. L., Allende Prieto, C. 2003, *MNRAS* 340, 304

- Reddy, B. E., Lambert, D. L., Allende Prieto, C., 2006, *MNRAS* 367, 1329
- Reddy, A. B. S., Giridhar, S., Lambert, D. L., 2012, *MNRAS* 419, 1350
- Richards, J. W., Starr, D. L., Miller, A. A., Bloom, J. S., Butler, N. R., Brink, H., Crellin-Quick, A., 2012, *ApJS* 203, 32
- Rodgers, A. W., Bell, R. A., 1963, *MNRAS* 125, 487
- Rodgers, A. W., Bell, R. A., 1968, *MNRAS* 1395, 75
- Sahin, T., Lambert, D. L., Klochkova, V. G., Tavganskaya, N. S., 2011, *MNRAS* 410, 612
- Samus N. N., Durlevich O. V., Kazarovets E. V., Kireeva N. N., Pastukhova E. N., Zharova A. V., et al, General Catalog of Variable Stars (GCVS database, Version 2013 Apr.)
- Sanford, R. F., 1953, *Trans. IAU*, 8, 809
- Savage, B. D., Sembach, K. R., 1996, *ARA&A* 34, 279
- Schmidt, E. G., Johnston, D., Langan, S., Lee, K. M., 2004, *AJ* 128, 1748
- Schmidt, E. G., Johnston, D., Langan, S., Lee, K. M., 2005, *AJ* 130, 832
- Schönrich, R., Binney, J., Dehnen, W., 2010, *MNRAS* 403, 1829
- Schwarzschild, M., 1953, *Trans. IAU*, 8, 811
- Skrutskie, M. F., Cutri, R. M., Stiening, R., Weinberg, M. D., Schneider, S., Carpenter, J. M., Beichman, C., Capps, R., Chester, T., Elias, J., Huchra, J., Liebert, J., Lonsdale, C., Monet, D. G., Price, S., Seitzer, P., Jarrett, T., Kirkpatrick, J. D., Gizis, J. E., Howard, E., Evans, T., Fowler, J., Fullmer, L., Hurt, R., Light, R., Kopan, E. L., Marsh, K. A., McCallon, H. L., Tam, R., Van Dyk, S., Wheelock, S., 2006, *AJ* 131, 1163
- Soszyński, I., Udalski, A., Szymański, M. K., Kubiak, M., Pietrzyński, G., Wyrzykowski, L., Szewczyk, O., Ulaczyk, K., Poleski, R., 2008, *AcA* 58, 293
- Tsymbal, V. V., 1996, *ASP Conf. Ser.*, 108, M.A.S.S.; *Model Atmospheres and Spectrum Synthesis*, ed. S. J. Adelman, F. Kupka & W. W. Weiss, 198.
- Wallerstein, G., 1958, *ApJ* 127, 583
- Wallerstein, G., 1959, *ApJ* 130, 560
- Wallerstein, G., Gonzalez, G., 1996, *MNRAS* 282, 1236
- Wallerstein, G., Matt, S., Gonzalez, G., 1996, *MNRAS* 311, 414
- Wallerstein, G., 2002, *PASP* 114, 689
- Wallerstein, G., Kovtyukh, V. V., Andrievsky, S. M., 2008, *PASP* 120, 361
- Waters, L. B. F. M., Trams, N. R., Waelkens, C., 1992, *A&A* 262, 37
- Watson C. L., 2006, *SASS* 25, 47
- Whitney, C. A., 1956a, *AnAp* 19, 34
- Whitney, C. A., 1956b, *AnAp* 19, 142
- Whitney, C. A., Scalafuris, A., 1963, *ApJ* 138, 200
- Yong, D., Carney, B. W., Teixeira de Almeida, M. L., Pohl, B. L., 2006, *AJ* 131, 2256
- Zacharias, N., Monet, D. G., Levine, S. E., Urban, S. E., Gaume, R., Wycoff, G. L., 2004, *AAS* 205, 48.15, 1418

Appendix A: An alternative approach to determining V_t

In this Appendix we show the standard deviation around the mean abundance plotted as a function of the microturbulent velocity, following the approach of Sahin et al. (2011). The dispersion of the abundances is computed for the Fe I, Fe II, Si I, and Ni I lines, while the microturbulent velocity V_t is varied from 1 to 6 km/s. The minimum value of the dispersion is in good agreement within the different elements, confirming the values of the microturbulence (derived solely from Fe I) adopted in this study, namely 3.1 km/s for HQ Car and 3.8 km/s for DD Vel..

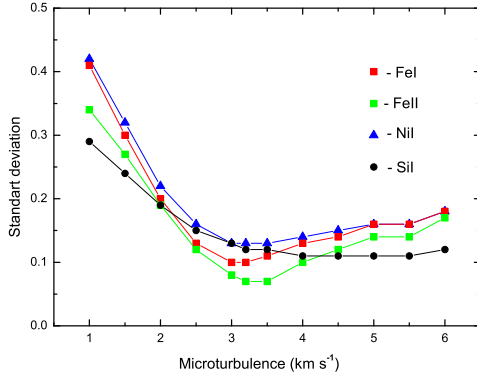


Fig. A.1: Standard deviation around the mean abundances as a function of microturbulence V_t for HQ Car, shown for several elements.

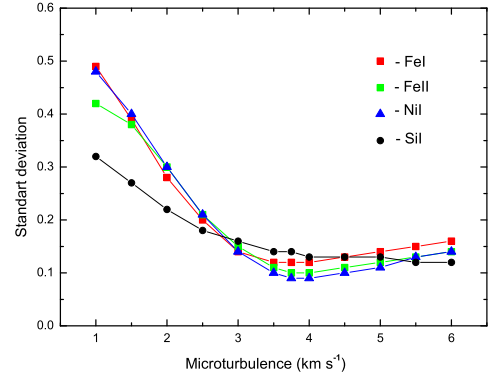


Fig. A.2: Same as Fig. A.1, but for DD Vel.

Appendix B: Solar references

Table B.1: Solar abundance derived from the solar spectrum using the grid of models by Castelli & Kurucz (2004), compared to the solar photospheric abundance by Asplund et al. (2009) and by Reddy et al. (2003).

Element	Log A (this work) dex	Lines used	Log A (Asplund et al. 2009) dex	Log A (Reddy et al. 2003) dex
C I	8.53±0.14	4	8.43±0.05	8.51±0.06
N I	8.15	2	7.83±0.05	8.06
O I	8.98	1	8.69±0.05	8.86±0.05
Na I	6.32±0.04	10	6.24±0.04	6.27
Mg I	7.68±0.02	9	7.60±0.04	7.54±0.06
Al I	6.30±0.01	2	6.45±0.03	6.28±0.05
Si I	7.55±0.08	23	7.51±0.03	7.62±0.05
S I	7.20±0.10	6	7.12±0.03	7.34±0.09
Ca I	6.32±0.07	16	6.34±0.04	6.33±0.07
Sc I			3.15±0.04	
Sc II	3.22±0.11	14		3.24±0.14
Ti I	4.96±0.08	41	4.95±0.05	4.90±0.06
Ti II	5.01±0.03	5		
V I	4.04±0.12	36	3.93±0.08	3.93±0.03
Cr I	5.67±0.09	23	5.64±0.04	5.68±0.07
Mn I	5.54±0.07	11	5.43±0.05	5.37±0.05
Fe I	7.57±0.08	164	7.50±0.04	7.45±0.04
Fe II	7.47±0.04	11		7.45±0.07
Co I	5.00±0.10	28	4.99±0.07	4.93±0.04
Ni I	6.29±0.06	56	6.22±0.04	6.23±0.04
Cu I	4.29±0.20	3	4.19±0.04	4.19±0.05
Zn I	4.45	1	4.56±0.05	4.47
Y II	2.15±0.17	7	2.21±0.05	2.12±0.04
Zr I			2.58±0.04	
Zr II	2.79±0.19	2		2.45
La II	1.24±0.02	2	1.10±0.04	
Ce II	1.70±0.11	6	1.58±0.04	1.58
Nd II	1.54±0.08	11	1.42±0.04	1.50
Eu II	0.96	1	0.52±0.04	0.61

Appendix A: List of lines used

Table A.1: Atomic parameters and EWs of HQ Car and DD Vel

Wavelength Å	Z	Log gf	χ_{ex} eV	HQ Car EW(mÅ)	DD Vel EW(mÅ)
6587.6100	6.00	-1.002	8.537	58.2	33.6
7087.8300	6.00	-1.441	8.647	27.8	...
7111.4700	6.00	-1.084	8.640	26.6	34.6
7113.1800	6.00	-0.772	8.647	51.6	...
7115.1700	6.00	-0.933	8.643	51.6	...
7116.9900	6.00	-0.906	8.647	71.4	...
7119.6600	6.00	-1.147	8.643	49.8	...
7442.2980	7.00	-0.400	10.330	13.8	24.8
7468.3120	7.00	-0.182	10.336	31.2	26.6
6300.3040	8.00	-9.818	0.000	107.9	...
6363.7760	8.00	-10.302	0.020	52.2	27.1
5682.6330	11.00	-0.705	2.102	105.8	97.6
5688.2050	11.00	-0.451	2.104	...	141.9
6154.2260	11.00	-1.546	2.102	32.6	29.0
6160.7470	11.00	-1.245	2.104	45.6	38.1
5711.0880	12.00	-1.723	4.346	132.2	123.4
6696.0230	13.00	-1.346	3.143	27.4	...
6698.6730	13.00	-1.646	3.143	8.4	...
7835.3090	13.00	-0.648	4.022	26.0	...
7836.1340	13.00	-0.493	4.022	18.5	...
5645.6130	14.00	-2.139	4.930	52.7	38.9
5665.5540	14.00	-2.039	4.920	53.4	37.7
5684.4840	14.00	-1.649	4.954	...	102.8
5690.4250	14.00	-1.869	4.930	81.8	51.5
5708.4000	14.00	-1.469	4.954	...	110.1
5772.1460	14.00	-1.749	5.082	...	60.8
5793.0730	14.00	-2.059	4.930	63.4	64.5
5948.5410	14.00	-1.229	5.082	...	114.2
6091.9190	14.00	-1.462	5.871	25.4	30.6
6106.6080	14.00	-1.896	5.614	21.2	...
6125.0210	14.00	-1.464	5.614	44.3	31.2
6131.8520	14.00	-1.616	5.616	41.6	...
6145.0160	14.00	-1.310	5.616	46.6	37.6
6155.1340	14.00	-0.754	5.619	117.4	...
6237.3190	14.00	-0.974	5.614	87.2	62.4
6243.8150	14.00	-1.243	5.616	71.9	44.6
6244.4650	14.00	-1.090	5.616	56.8	...
6414.9800	14.00	-1.035	5.871	66.5	45.9
6526.6300	14.00	-1.606	5.871	...	22.3
6721.8480	14.00	-1.526	5.863	...	37.4
6800.5960	14.00	-1.944	5.964	14.3	...
6848.5800	14.00	-1.527	5.863	21.5	...
7034.9010	14.00	-0.879	5.871	...	68.5
7226.2080	14.00	-1.509	5.614	...	31.3
7282.8160	14.00	-0.625	6.206	69.9	78.6
7373.0040	14.00	-1.179	5.984	34.0	...
7424.6100	14.00	-1.609	5.619	24.0	...
7680.2660	14.00	-0.689	5.863	...	95.5
7918.3830	14.00	-0.609	5.954	100.9	...
7932.3480	14.00	-0.469	5.964	107.0	...
7944.0010	14.00	-0.309	5.984	128.8	...
6347.1090	14.01	0.170	8.121	166.4	132.4
6371.3710	14.01	-0.039	8.121	...	93.5
6045.9720	16.00	-1.317	7.868	44.8	29.0
6045.9920	16.00	-1.907	7.868	44.8	29.0
6046.0380	16.00	-1.113	7.868	44.8	29.0
6743.5800	16.00	-0.849	7.866	52.5	...

Table A.1: continued.

Wavelength Å	Z	Log gf	χ_{ex} eV	HQ Car EW(mÅ)	DD Vel EW(mÅ)
6748.7900	16.00	-0.529	7.868	68.8	33.9
6757.1500	16.00	-0.239	7.870	83.6	41.4
7686.1010	16.00	-0.987	7.868	26.8	...
5349.4650	20.00	-0.309	2.709	...	106.3
5512.9800	20.00	-0.463	2.933	...	60.7
5581.9650	20.00	-0.554	2.523	104.4	91.8
5590.1140	20.00	-0.570	2.521	97.3	88.4
5601.2770	20.00	-0.522	2.526	133.2	104.2
5867.5620	20.00	-1.569	2.933	22.4	...
6161.2970	20.00	-1.265	2.523	42.9	37.7
6166.4390	20.00	-1.141	2.521	52.8	43.5
6169.0420	20.00	-0.796	2.523	...	74.2
6169.5630	20.00	-0.477	2.526	106.2	103.6
6449.8080	20.00	-0.501	2.521	...	111.2
6471.6620	20.00	-0.685	2.526	122.6	90.0
6493.7810	20.00	-0.108	2.521	...	162.1
6499.6500	20.00	-0.817	2.523	86.3	77.9
6717.6810	20.00	-0.523	2.709	...	105.9
7326.1450	20.00	-0.207	2.933	...	98.5
5020.0260	22.00	-0.413	0.836	...	94.1
5022.8680	22.00	-0.433	0.826	...	80.9
5024.8440	22.00	-0.601	0.818	...	68.5
5036.4640	22.00	0.130	1.443	...	90.0
5039.9570	22.00	-1.089	0.021	...	83.0
5210.3850	22.00	-0.849	0.048	...	110.8
5224.3000	22.00	0.130	2.134	...	37.2
5514.5330	22.00	-0.359	1.443	...	38.0
5644.1330	22.00	0.231	2.267	50.2	31.8
5866.4510	22.00	-0.839	1.067	35.7	33.1
6098.6580	22.00	-0.009	3.062	9.7	...
6126.2160	22.00	-1.424	1.067	16.0	...
6258.1020	22.00	-0.354	1.443	...	43.2
6258.7060	22.00	-0.239	1.460	59.7	51.3
6261.0970	22.00	-0.478	1.430	44.7	36.8
5005.1570	22.01	-2.729	1.566	...	98.3
5268.6150	22.01	-1.669	2.598	...	109.8
5381.0150	22.01	-1.969	1.566
5396.2260	22.01	-3.019	1.584	...	52.3
5418.7510	22.01	-2.109	1.582
6606.9500	22.01	-2.789	2.061	63.8	39.9
5670.8530	23.00	-0.419	1.081	19.7	...
5698.5190	23.00	-0.110	1.064	35.1	30.4
5703.5750	23.00	-0.210	1.051	23.2	...
5727.0480	23.00	-0.011	1.081	25.8	29.2
5731.2410	23.00	-0.729	1.064	14.0	...
6090.2140	23.00	-0.061	1.081	...	33.4
6111.6450	23.00	-0.714	1.043	10.7	...
6199.1970	23.00	-1.299	0.287	19.9	19.8
6216.3540	23.00	-1.289	0.275	23.8	...
6242.8290	23.00	-1.549	0.262	13.1	...
5819.9250	23.01	-1.692	2.522	29.8	...
5928.8520	23.01	-1.682	2.522	42.8	...
5247.5650	24.00	-1.589	0.961	...	91.8
5296.6910	24.00	-1.359	0.983	...	116.8
5297.3770	24.00	0.209	2.900	...	67.0
5329.1380	24.00	-0.007	2.914	...	50.3
5348.3150	24.00	-1.209	1.004	...	125.1
5783.8500	24.00	-0.360	3.322	18.6	...
5787.9180	24.00	-0.049	3.322	28.6	29.1
6661.0750	24.00	-0.112	4.193	11.7	...

Table A.1: continued.

Wavelength Å	Z	Log gf	χ_{ex} eV	HQ Car EW(mÅ)	DD Vel EW(mÅ)
7400.2490	24.00	-0.049	2.900		64.2
5237.3280	24.01	-1.349	4.073	...	160.9
5310.6860	24.01	-2.407	4.072	...	46.2
5313.5630	24.01	-1.778	4.074	...	115.3
5334.8690	24.01	-1.825	4.072	...	107.4
5407.6040	24.01	-2.150	3.827	...	82.5
5502.0670	24.01	-2.116	4.168	...	53.3
5508.6060	24.01	-2.251	4.156	...	56.1
5002.7930	26.00	-1.579	3.397	...	107.3
5004.0440	26.00	-1.399	4.209	...	50.3
5022.2360	26.00	-0.529	3.984	...	142.9
5029.6180	26.00	-2.049	3.415	...	53.9
5044.2110	26.00	-2.037	2.851	...	91.5
5048.4360	26.00	-1.029	3.960	...	83.1
5054.6430	26.00	-1.920	3.640	...	48.8
5060.0360	26.00	-1.147	4.301	...	74.6
5060.0790	26.00	-5.459	0.000	...	74.6
5067.1500	26.00	-0.969	4.220	...	84.8
5090.7740	26.00	-0.399	4.256	...	128.9
5109.6520	26.00	-0.979	4.301	...	94.6
5131.4690	26.00	-2.514	2.223	...	141.0
5159.0580	26.00	-0.819	4.283	...	89.6
5180.0700	26.00	-1.259	4.473	...	40.1
5187.9140	26.00	-1.370	4.143	...	49.3
5225.5260	26.00	-4.788	0.110	...	132.8
5228.3770	26.00	-1.289	4.220	...	58.7
5242.4910	26.00	-0.966	3.634	...	120.9
5243.7770	26.00	-1.149	4.256	...	65.9
5247.0500	26.00	-4.945	0.087	...	130.4
5253.4620	26.00	-1.572	3.283	...	99.4
5288.5250	26.00	-1.507	3.695	...	56.8
5307.3610	26.00	-2.986	1.608	...	151.2
5322.0410	26.00	-2.802	2.279	...	78.3
5329.9890	26.00	-1.188	4.076	...	58.6
5353.3740	26.00	-0.839	4.103	...	121.8
5373.7090	26.00	-0.859	4.473	...	66.3
5379.5740	26.00	-1.513	3.695	...	59.2
5389.4790	26.00	-0.409	4.415	...	110.1
5398.2790	26.00	-0.669	4.446	...	82.3
5409.1340	26.00	-1.299	4.371	...	52.4
5441.3390	26.00	-1.729	4.313	...	20.7
5464.2800	26.00	-1.401	4.143	...	34.2
5466.3960	26.00	-0.629	4.371	...	95.5
5473.9010	26.00	-0.759	4.154	...	100.1
5481.2430	26.00	-1.242	4.103	...	77.5
5487.7450	26.00	-0.316	4.320	...	129.9
5522.4470	26.00	-1.549	4.209	...	35.4
5543.1500	26.00	-1.569	3.695		66.6
5543.9360	26.00	-1.139	4.218	67.6	69.9
5546.5060	26.00	-1.309	4.371	56.7	51.1
5554.8950	26.00	-0.439	4.549	104.4	...
5560.2120	26.00	-1.189	4.435	54.4	50.7
5563.6000	26.00	-0.989	4.191	...	99.9
5565.7040	26.00	-0.212	4.608	118.1	105.0
5567.3910	26.00	-2.563	2.609	83.1	67.9
5576.0890	26.00	-0.999	3.430	147.5	...
5584.7650	26.00	-2.319	3.573	26.1	29.3
5618.6330	26.00	-1.275	4.209	51.9	42.7
5619.5950	26.00	-1.699	4.387	32.7	...
5633.9470	26.00	-0.269	4.991	86.7	72.6

Table A.1: continued.

Wavelength Å	Z	Log gf	χ_{ex} eV	HQ Car EW(mÅ)	DD Vel EW(mÅ)
5638.2620	26.00	-0.869	4.220	101.3	...
5650.7060	26.00	-0.959	5.086	...	30.5
5651.4690	26.00	-1.999	4.473	15.7	...
5652.3180	26.00	-1.949	4.260	24.5	...
5653.8670	26.00	-1.639	4.387	33.3	30.6
5661.3460	26.00	-1.735	4.284	18.7	...
5662.5160	26.00	-0.572	4.178	...	126.5
5679.0230	26.00	-0.919	4.652	54.5	54.7
5686.5300	26.00	-0.445	4.549	96.4	80.6
5691.4970	26.00	-1.519	4.301	44.1	29.0
5701.5450	26.00	-2.215	2.559	131.4	126.4
5705.9920	26.00	-0.529	4.608	...	93.5
5717.8330	26.00	-1.129	4.284	76.0	64.0
5731.7620	26.00	-1.299	4.256	62.2	55.2
5741.8480	26.00	-1.853	4.256	19.4	23.1
5752.0320	26.00	-1.176	4.549	54.8	51.6
5753.1230	26.00	-0.687	4.260	108.3	100.0
5762.9920	26.00	-0.449	4.209	...	142.9
5775.0810	26.00	-1.297	4.220	61.7	56.6
5784.6580	26.00	-2.531	3.397	...	22.0
5793.9150	26.00	-1.699	4.220	24.6	34.5
5806.7250	26.00	-1.049	4.608	51.2	45.6
5809.2180	26.00	-1.839	3.884	43.5	44.2
5814.8080	26.00	-1.969	4.283	15.7	...
5816.3740	26.00	-0.600	4.549	80.5	...
5852.2190	26.00	-1.329	4.549	36.1	24.5
5859.5860	26.00	-0.418	4.549	89.2	...
5862.3560	26.00	-0.126	4.549	122.6	109.6
5883.8170	26.00	-1.359	3.960	82.6	69.0
5905.6720	26.00	-0.729	4.652	58.4	53.6
5909.9740	26.00	-2.586	3.211	...	45.0
5916.2470	26.00	-2.993	2.453	...	67.9
5927.7890	26.00	-1.089	4.652	36.0	...
5930.1800	26.00	-0.229	4.652	117.9	116.0
5934.6550	26.00	-1.169	3.929	101.9	86.0
5952.7180	26.00	-1.439	3.984	75.5	58.4
5956.6940	26.00	-4.604	0.859	...	63.4
5976.7770	26.00	-1.242	3.943	90.0	75.3
5984.8150	26.00	-0.195	4.733	106.2	95.3
5987.0650	26.00	-0.428	4.796	80.3	...
6003.0120	26.00	-1.119	3.882	117.7	97.2
6007.9600	26.00	-0.596	4.652	70.8	60.0
6008.5560	26.00	-0.985	3.884	121.8	109.3
6020.1690	26.00	-0.269	4.608	...	131.0
6024.0580	26.00	-0.119	4.549	...	153.4
6027.0510	26.00	-1.088	4.076	80.8	77.5
6056.0050	26.00	-0.459	4.733	91.8	74.3
6062.8480	26.00	-4.139	2.176	17.9	...
6078.4910	26.00	-0.320	4.796	97.2	82.4
6082.7110	26.00	-3.572	2.223	40.7	31.9
6085.2590	26.00	-3.094	2.759	33.3	...
6093.6440	26.00	-1.499	4.608	30.1	...
6096.6650	26.00	-1.929	3.984	40.8	34.4
6098.2450	26.00	-1.879	4.559	17.0	...
6127.9070	26.00	-1.398	4.143	43.3
6151.6180	26.00	-3.298	2.176	65.3	59.4
6157.7280	26.00	-1.259	4.076	79.3	62.6
6165.3600	26.00	-1.473	4.143	39.1
6170.5070	26.00	-0.439	4.796	91.3	77.4
6173.3360	26.00	-2.879	2.223	99.9	89.8

Table A.1: continued.

Wavelength Å	Z	Log gf	χ_{ex} eV	HQ Car EW(mÅ)	DD Vel EW(mÅ)
6180.2040	26.00	-2.585	2.728	67.3	62.8
6187.9900	26.00	-1.719	3.943	43.6	45.2
6200.3130	26.00	-2.436	2.609	102.7	96.9
6213.4300	26.00	-2.481	2.223	140.4	131.6
6215.1440	26.00	-1.319	4.186	73.8	...
6219.2810	26.00	-2.432	2.198	...	158.5
6220.7840	26.00	-2.459	3.882	18.4	...
6226.7360	26.00	-2.219	3.884	24.3	...
6229.2280	26.00	-2.804	2.845	56.1	44.5
6232.6410	26.00	-1.222	3.654	102.7	96.9
6240.6460	26.00	-3.232	2.223	60.1	49.6
6246.3190	26.00	-0.732	3.603	161.7	153.7
6256.3620	26.00	-2.407	2.453	...	134.5
6265.1340	26.00	-2.549	2.176	...	134.7
6271.2790	26.00	-2.702	3.332	25.1	...
6290.9650	26.00	-0.773	4.733	...	54.6
6297.7930	26.00	-2.739	2.223	...	101.4
6301.5010	26.00	-0.717	3.654	...	161.6
6311.5000	26.00	-3.140	2.832	36.8	24.9
6322.6860	26.00	-2.425	2.588	107.2	96.1
6336.8240	26.00	-0.855	3.686	147.0	132.2
6344.1490	26.00	-2.922	2.433	69.7	72.1
6355.0290	26.00	-2.349	2.845	92.4	79.3
6358.6980	26.00	-4.467	0.859	105.4	100.7
6364.3660	26.00	-1.429	4.796	26.5	...
6380.7430	26.00	-1.375	4.186	50.7	45.6
6392.5390	26.00	-4.029	2.279	16.7	...
6408.0180	26.00	-1.017	3.686	135.9	...
6419.9500	26.00	-0.239	4.733	109.5	88.6
6475.6240	26.00	-2.941	2.559	81.2	61.7
6481.8700	26.00	-2.983	2.279	...	82.7
6498.9390	26.00	-4.698	0.958	55.7	51.7
6518.3670	26.00	-2.459	2.832	74.6	63.2
6533.9290	26.00	-1.459	4.559	28.4	29.8
6593.8710	26.00	-2.421	2.433	123.2	112.1
6597.5610	26.00	-1.069	4.796	40.8	44.6
6609.1100	26.00	-2.691	2.559	78.1	71.9
6625.0220	26.00	-5.349	1.011	23.6	...
6627.5450	26.00	-1.679	4.549	21.3	...
6663.4420	26.00	-2.478	2.424	...	127.2
6703.5670	26.00	-3.159	2.759	30.9	30.5
6710.3200	26.00	-4.879	1.485	14.7	...
6715.3830	26.00	-1.639	4.608	18.7	...
6725.3570	26.00	-2.299	4.103	14.1	...
6726.6660	26.00	-1.132	4.607	39.8	32.2
6733.1510	26.00	-1.579	4.638	24.6	17.4
6739.5220	26.00	-4.793	1.557	12.4	...
6750.1530	26.00	-2.620	2.424	116.7	100.9
6752.7070	26.00	-1.203	4.638	29.9	...
6783.7040	26.00	-3.979	2.588	11.4	...
6786.8600	26.00	-2.069	4.191	24.2	...
6804.0010	26.00	-1.495	4.652	18.4	...
6806.8450	26.00	-3.209	2.728	37.9	33.1
6810.2630	26.00	-0.985	4.607	45.7	36.3
6820.3720	26.00	-1.319	4.638	28.5	32.7
6828.5910	26.00	-0.919	4.638	58.0	50.6
6837.0060	26.00	-1.686	4.593	19.7	...
6839.8310	26.00	-3.449	2.559	30.3	23.8
6841.3390	26.00	-0.749	4.607	85.3	61.9
6842.6860	26.00	-1.319	4.638	33.9	27.5

Table A.1: continued.

Wavelength Å	Z	Log gf	χ_{ex} eV	HQ Car EW(mÅ)	DD Vel EW(mÅ)
6843.6560	26.00	-0.929	4.549	70.4	58.0
6855.1620	26.00	-0.741	4.559	...	75.4
6858.1500	26.00	-0.929	4.608	58.3	36.1
7024.6430	26.00	-1.079	4.559	...	38.0
7038.2230	26.00	-1.299	4.218	...	57.4
7068.4100	26.00	-1.379	4.076	71.6	54.8
7090.3840	26.00	-1.209	4.231	69.2	62.0
7127.5680	26.00	-1.045	4.988	24.8	...
7130.9220	26.00	-0.789	4.218	112.3	98.8
7132.9860	26.00	-1.627	4.076	...	32.5
7151.5000	26.00	-3.729	2.484	28.0	...
7189.1450	26.00	-2.770	3.071	49.0	31.1
7219.6850	26.00	-1.689	4.076	34.0	33.5
7284.8350	26.00	-1.749	4.143	29.8	32.6
7306.5620	26.00	-1.739	4.178	40.1	36.2
7351.5120	26.00	-0.636	4.956	52.7	...
7411.1530	26.00	-0.298	4.283	138.7	135.0
7440.9120	26.00	-0.572	4.913	...	44.5
7443.0220	26.00	-1.819	4.186	29.2	...
7461.5210	26.00	-3.579	2.559	22.8	...
7491.6470	26.00	-0.898	4.301	75.3	73.3
7568.8990	26.00	-0.772	4.283	...	76.7
7583.7880	26.00	-1.884	3.018	107.0	102.4
7586.0180	26.00	-0.457	4.313	...	151.2
7710.3650	26.00	-1.112	4.220	...	67.7
7748.2690	26.00	-1.750	2.949	150.6	141.3
7751.1090	26.00	-0.752	4.991	45.4	33.5
7780.5570	26.00	0.029	4.473	149.8	164.3
7807.9090	26.00	-0.540	4.991	52.6	...
7832.1950	26.00	0.111	4.435	...	171.1
7855.3990	26.00	-1.019	5.064	26.1	...
5120.3520	26.01	-4.255	2.828	...	90.7
5132.6690	26.01	-3.979	2.807	...	98.3
5161.1840	26.01	-4.572	2.856	...	49.0
5256.9370	26.01	-4.181	2.891	...	94.3
5414.0730	26.01	-3.539	3.221	...	128.4
5425.2570	26.01	-3.159	3.199	...	156.7
5627.4970	26.01	-4.129	3.387	...	57.4
5991.3760	26.01	-3.539	3.153	...	132.0
6084.1110	26.01	-3.779	3.199	...	96.5
6113.3220	26.01	-4.109	3.221	80.9	73.5
6149.2580	26.01	-2.719	3.889	...	143.1
6233.5340	26.01	-2.831	5.484	11.5	...
6369.4620	26.01	-4.159	2.891	...	100.9
6383.7220	26.01	-2.069	5.553	47.3	31.6
6416.9190	26.01	-2.649	3.892	...	145.9
6432.6800	26.01	-3.519	2.891	...	155.8
6442.9550	26.01	-2.670	5.549	...	17.7
6446.4100	26.01	-1.959	6.223	23.0	...
7222.3940	26.01	-3.359	3.889	...	84.8
7449.3350	26.01	-3.089	3.889	102.2	...
7479.6930	26.01	-3.679	3.892	55.7	44.7
7515.8310	26.01	-3.459	3.903	76.9	71.6
7711.7230	26.01	-2.499	3.903	161.8	...
5483.3530	27.00	-1.489	1.710	...	59.4
5647.2340	27.00	-1.559	2.280	23.0	...
6188.9960	27.00	-2.449	1.710	19.4	...
6771.0340	27.00	-1.969	1.883	15.4	16.5
6814.9440	27.00	-1.899	1.956	22.5	...
7084.9830	27.00	-1.114	1.883	70.4	54.9

Table A.1: continued.

Wavelength Å	Z	Log gf	χ_{ex} eV	HQ Car EW(mÅ)	DD Vel EW(mÅ)
5000.3430	28.00	-0.429	3.635	...	102.7
5003.7410	28.00	-2.799	1.676	...	50.3
5010.9380	28.00	-0.869	3.635	...	51.6
5032.7270	28.00	-1.269	3.898	...	15.5
5035.3570	28.00	0.290	3.635	...	162.8
5048.8470	28.00	-0.379	3.847	...	77.4
5080.5280	28.00	0.330	3.655	...	171.7
5081.1100	28.00	0.300	3.847	...	142.3
5082.3440	28.00	-0.539	3.658	...	77.1
5084.0960	28.00	0.030	3.679	...	133.1
5099.9300	28.00	-0.099	3.679	...	121.5
5115.3920	28.00	-0.109	3.834	...	108.1
5155.1260	28.00	-0.649	3.898	...	46.5
5155.7640	28.00	0.074	3.898	...	91.4
5176.5600	28.00	-0.439	3.898	...	57.7
5435.8580	28.00	-2.589	1.986	...	53.5
5578.7180	28.00	-2.639	1.676	69.6	63.3
5587.8580	28.00	-2.139	1.935	...	70.0
5593.7350	28.00	-0.839	3.898	49.7	35.5
5663.9850	28.00	-0.429	4.538	...	25.0
5694.9830	28.00	-0.609	4.089	...	37.4
5754.6560	28.00	-2.329	1.935	106.2	...
5760.8300	28.00	-0.799	4.105	34.0	...
5805.2170	28.00	-0.639	4.167	44.5	31.4
5831.5950	28.00	-0.944	4.167	25.3	21.3
5846.9930	28.00	-3.209	1.676	26.4	21.3
5996.7300	28.00	-1.059	4.236	16.2	...
6086.2810	28.00	-0.529	4.266	28.0	29.1
6108.1160	28.00	-2.449	1.676	88.7	90.4
6111.0700	28.00	-0.869	4.088	35.6	22.3
6128.9730	28.00	-3.329	1.676	28.2	...
6133.9630	28.00	-1.829	4.088	7.1	...
6175.3660	28.00	-0.529	4.089	67.2	48.6
6176.8070	28.00	-0.259	4.088	78.4	64.3
6204.6000	28.00	-1.099	4.088	21.6	...
6223.9810	28.00	-0.909	4.105	25.4	21.7
6259.5950	28.00	-1.236	4.089	17.4	...
6322.1660	28.00	-1.169	4.154	25.8	...
6327.5980	28.00	-3.149	1.676	42.4	37.7
6360.8110	28.00	-1.026	4.167	15.5	...
6366.4800	28.00	-0.873	4.167	17.7	...
6378.2470	28.00	-0.829	4.154	33.3	28.1
6532.8730	28.00	-3.389	1.935	23.9	...
6586.3100	28.00	-2.809	1.951	53.0	37.7
6598.5980	28.00	-0.979	4.236	30.4	...
6635.1220	28.00	-0.819	4.419	16.8	...
6767.7720	28.00	-2.169	1.826	137.5	120.5
6772.3150	28.00	-0.979	3.658	58.7	46.3
6914.5590	28.00	-2.269	1.951	...	86.3
7110.8960	28.00	-2.979	1.935	35.9	...
7122.1970	28.00	0.040	3.542	159.0	153.9
7181.9690	28.00	-0.739	3.743	79.3	74.4
7385.2370	28.00	-1.969	2.740	38.6	...
7422.2750	28.00	-0.139	3.635	134.7	139.5
7522.7590	28.00	-0.464	3.658	95.6	90.7
7525.1110	28.00	-0.432	3.635	99.8	82.1
7555.5970	28.00	0.054	3.847	129.3	120.0
7574.0420	28.00	-0.448	3.833	...	74.8
7797.5800	28.00	-0.184	3.898	102.9	97.1
4722.1530	30.00	-0.337	4.030	...	143.8

Table A.1: continued.

Wavelength Å	Z	Log gf	χ_{ex} eV	HQ Car EW(mÅ)	DD Vel EW(mÅ)
4810.5280	30.00	-0.136	4.078	...	163.0
5087.4160	39.01	-0.169	1.084	...	75.9
5200.4060	39.01	-0.569	0.992	...	54.1
5509.8950	39.01	-0.947	0.992	...	39.7
6613.7320	39.01	-0.847	1.748	27.6	...
6795.4140	39.01	-1.029	1.738	14.9	...
6407.2160	40.01	-2.699	0.154	55.7	...
6262.2900	57.01	-1.219	0.403	19.6	...
6320.3760	57.01	-1.609	0.173	19.8	...
6390.4800	57.01	-1.409	0.321	17.8	...
5092.7900	60.01	-0.609	0.380	...	32.3
5130.5900	60.01	0.450	1.304	...	32.5
5740.8600	60.01	-0.529	1.160	11.5	...
6645.0940	63.01	-0.161	1.380	66.5	...